International Journal of Materials Chemistry and Physics
Vol. 1, No. 3, 2015, pp. 286-294
http://www.aiscience.org/journal/ijmcp

Features of Crystal Structure and Magnetic Properties of M-type Ba-hexaferrites with Diamagnetic Substitution

A. V. Trukhanov[1, 2, *], L. V. Panina[1], S. V. Trukhanov[2], V. O. Turchenko[3], I. S. Kazakevich[2], M. M. Salem[1]

[1]Department of Electronic Materials Technology, National University of Science and Technology MISiS, Moscow, Russia
[2]Laboratory of magnetic films physics, SSPA "Scientific and practical materials research centre of NAS of Belarus", Minsk, Belarus
[3]Laboratory of Neutron Physics, Joint Institute for Nuclear Research, Dubna, Russia

Abstract

The investigations of the crystal and magnetic structure by powder neutron diffractometry as well as the magnetic properties by vibration sample magnetometry for the $BaFe_{12-x}Al_xO_{19}$ (x=0.1-1.2) solid solutions have been performed at different temperatures and magnetic fields. The atomic coordinates and lattice parameters have been Rietveld refined. The Invar effect has been observed in low temperature range (from 150 to 4.2 K). It was explained by the thermal oscillation anharmonicity of atoms. The increase of microstress value with decreasing temperature has been defined from Rietveld refinement. The Curie temperature and change of total magnetic moment per formula unit have been defined for all the compositions of the barium hexaferrites $BaFe_{12-x}Al_xO_{19}$ (x=0.1-1.2) solid solutions. The magnetic structure model is proposed. The most likely reasons and the mechanism of magnetic structure formation are discussed.

Keywords

Barium Hexaferrites, Neutron Diffraction, Crystal and Magnetic Structures

Received: August 24, 2015 / Accepted: September 19, 2015 / Published online: October 16, 2015

1. Introduction

The barium and strontium hexaferrites and the solid solutions on their base which doped by Al^{3+}, Sc^{3+}, In^{3+} and Ga^{3+} ions [1, 2] attract much attention of researches [3-5] due to their unique physical properties. They provide a wide range of potential applications, such as multiple-state memory elements, novel memory media, transducers and new functional sensors are needed. The barium ferrite with hexagonal structure and molecular formula $BaFe_{12}O_{19}$ has a magnetoplumbite (M) structure which was determined by Adelsklod [6] in 1938. The unit cell, which includes two formula units (Z=2), contains 38 oxygen ions, 24 iron ions and 2 barium ions [7]. The iron ions occupy the nine 6-fold octahedral sites (12k, 2a and $4f_{VI}$), the one 5-fold trigonal site (2b) and the two 4-fold tetrahedral sites ($4f_{IV}$). The barium ions occupy 2d sites. The spin orientations of each sites are: for the $4f_{IV}$ and $4f_{VI}$ sites spin is down; for the 2a, 2b and 12k sites spin is up. The hexaferrites have large magnetocrystalline anisotropy, high Curie temperature, relatively large magnetization, as well as its excellent chemical stability and corrosion resistivity. The value of anisotropy energy constant such materials exceed values of garnet ferrites in a hundred times more. Such excellent functional properties made it possible their practical applications as permanent magnets [8], magnetic recording media [9], and microwave devices. Hexagonal ferrites are successful used in absorption of centimetric radio waves. Such technology is well known as "Stealth" technology. Recently was reported that Co/Ti-substituted hexagonal M-

* Corresponding author
E-mail address: truhanov86@mail.ru (A. V. Trukhanov)

type ferrite is an excellent material for the high-frequency multilayer inductors [10].

It is interesting that the materials in which ferroelectricity and ferromagnetism coexist are rare [11] and mostly provide rather weak ferromagnetism. Because the multiferroism at room temperature is an essential issue for the realization of multiferroic devices that exploit the coupling between ferroelectric and ferromagnetic orders at ambient conditions, $BiFeO_3$ [12] together with recently investigated $LuFe_2O_4$ [13], $Pb_2Fe_2O_5$ [14] and $PbFe_{12}O_{19}$ [15] is currently considered to be promising candidates for device applications. The perovskite $BiFeO_3$ [12] shows weak magnetism, which somehow limit its practical application. Therefore, preparation of a material in which large ferroelectricity and strong ferromagnetism coexist would be a milestone for modern electrics and functionalized materials [16]. Since large ferroelectric polarization was found in $PbFe_{12}O_{19}$ ceramics [15] with hexagonal structure, it opened a new direction for potential multiferroic candidate to the conventional ferromagnetic oxides, such as $BaFe_{12}O_{19}$, which holds similar perovskite-like lattice units in its hexagonal structure.

As earlier studies have shown [17] the $BaFe_{12}O_{19}$ is a perspective Pb-free multiferroic material. The large spontaneous polarization was observed for the $BaFe_{12}O_{19}$ ceramics at room temperature, revealing a clear ferroelectric hysteresis loop. The maximum remanent polarization was estimated approximately 11.8 $\mu C/cm^2$. The FeO_6 octahedron in its perovskite-like hexagonal unit cell and the shift of Fe^{3+} off the center of octahedron are suggested to be the origin of the polarization in $BaFe_{12}O_{19}$. The magnetic field induced electric polarization has been also observed in the doped $BaFe_{12-x-\delta}Sc_xM_\delta O_{19}$ (δ=0.05) at 10 K [18].

The presence of magnetically ordered state and ferroelectric properties open new opportunity for wide practical application of the hexaferrites. The key point for such applications is controlling the magnetic properties of these materials. The analysis of experimental data of multicomponent oxides so as the hexaferrites shows that they physical properties are directly depended on concentration of diamagnetic substitution [19], type of crystal structure, crystalline size [20] and even anion stoichiometry [21, 22]. The detailed study of the crystal structure and magnetic properties for the $BaFe_{12-x}Al_xO_{19}$ (x=0.1-1.2) solid solutions are present and discussed in present paper.

2. Experiment

The investigated $BaFe_{12-x}Al_xO_{19}$ (x=0.1; 0.3; 0.6; 09 and 1.2) samples have been obtained from high purity Fe_2O_3 and Al_2O_3 oxides and carbonate $BaCO_3$ using 'two-steps' topotactic reactions (conventional solid reaction method). At first the oxides and carbonate have been mixed with design ratio. Then the prefiring has been performed at 1200°C in air during 6 h. Final synthesis was carried out at 1300°C in air during 6 h. After synthesis the sample has been slowly cooled (100°C*h^{-1}). The formation of $BaFe_{12-x}Al_xO_{19}$ powder can be represented as follows:

$$BaCO_3 + \left(6 - \frac{1}{2}x\right)Fe_2O_3 + \left(\frac{1}{2}x\right)Al_2O_3 \rightarrow BaFe_{12-x}Al_xO_{19} + CO_2\uparrow \quad (1)$$

The powder neutron investigations of solid solutions were performed by neutron time of flight method at High Resolution Fourier Diffractometer (HRFD, Dubna) in broad temperature range (4.2–730 K). The refining of crystal and magnetic structures was performed by Rietveld analysis [23], using the FullProf [24] software program. The resolution of diffractometer is $\Delta d/d \sim 0.001\%$ and lattice parameters were defined more exactly at standard Al_2O_3 (standard SRM-676 of NIST, USA). For obtaining low and high temperatures were used facilities of Sumitomo Heavy Industries Ltd. firm and of Eurotherm firm, consequently. Field dependences of specific magnetization were measured at 300 K by Liquid Helium Free High Field Measurement System (VSM). The Curie temperature was defined in temperature range of 300–800 K and in magnetic field of 0.86 T. The phase transition temperature "ferromagnetic-paramagnetic" for $BaFe_{12-x}Al_xO_{19}$ has been defined as the inflection point in the temperature dependence of the specific magnetization.

3. Results and Discussion

3.1. Crystal Structure

According to neutron data the investigated samples possess a hexagonal structure with space group ($P6_3/mmc$) with two molecules in the unit cell (Z = 2). The powder neutron diffraction pattern for the $BaFe_{11.7}Al_{0.3}O_{19}$ is presented on Fig. 1.

An impurity hematite phase Fe_2O_3 is also present with space group (R-3c), with six molecules in the unit cell (Z = 6), similarly to [25, 26]. This is the result of slight dissolution of the $BaO*Fe_2O_3$ (tetragonal lattice) in the M-type hexaferrite. The impurity phase formation fact can be eliminated by introducing the synthesis of a small amount (0.4 mol%.) BaO.

The R_{wp} (weighted profile R-value), R_{exp} (expected R-value), R_B- (Bragg R-factor), R_{Mag} (magnetic R-factor) and χ^2 (goodness-of-fit quality factor) parameters [27] obtained after refinement are presented in Table 1. The low values of fitting parameters suggest that the studied sample is of better quality and refinements of neutron data are effective.

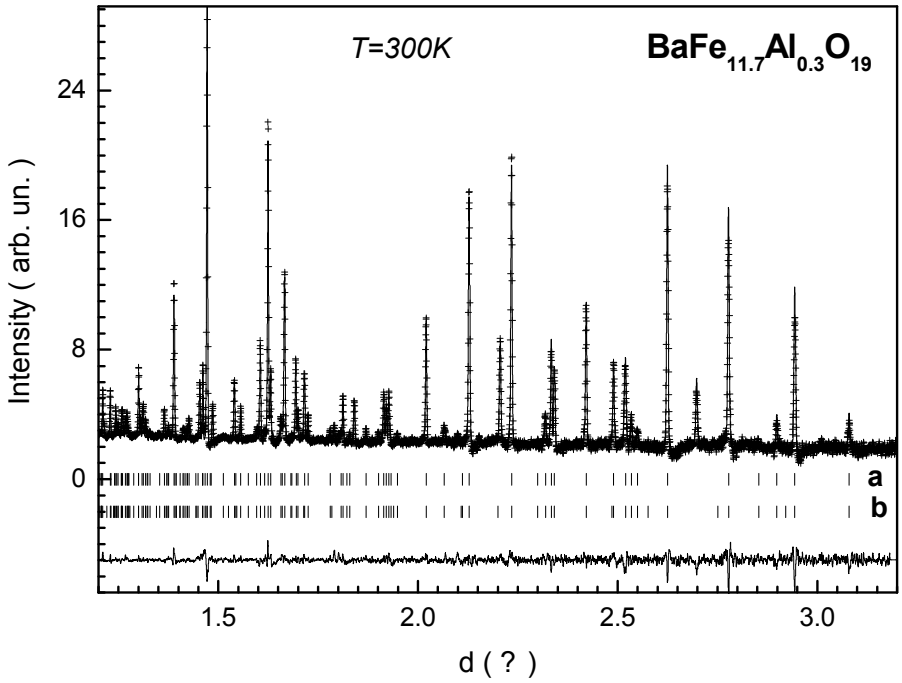

Fig. 1. Powder neutron diffraction pattern for the $BaFe_{11.7}Al_{0.3}O_{19}$ sample, measured at 300 K and calculated by Rietveld method. It is shown the experimental points (crosses), calculated function (curve), difference curve (lower curve) and diffraction peak positions (vertical bars) for the atomic (a) and magnetic (b) structure of the $BaFe_{11.7}Al_{0.3}O_{19}$.

Table 1. The crystal structure parameters obtained by powder neutron diffraction at 300 K for the $BaFe_{12-x}Al_xO_{19}$ (x = 0.1–1.2) solid solutions.

x / atom parameters	0.1	0.3	0.6	0.9	1.2
a, (Å)	5.8899(2)	5.8854(1)	5.8846(1)	5.8809(2)	5.8700(2)
c, (Å)	23.1972(6)	23.1756(5)	23.1719(3)	23.1686(9)	23.1268(9)
V, (Å^3)	696.91(3)	695.21(2)	694.91(2)	693.93(5)	690.12(4)
Fe3/Al3 ($4f_{IV}$)					
z	0.02741(16)	0.02717(17)	0.02771(17)	0.02780(24)	0.02815(30)
Fe4/Al4 ($4f_{VI}$)					
z	0.18898(12)	0.18996(13)	0.19008(13)	0.18908(18)	0.19005(24)
Fe5/Al5 (12k)					
x	0.16689(43)	0.16768(49)	0.16715(42)	0.16724(62)	0.16893(84)
z	-0.10829(5)	-0.10812(5)	-0.10805(6)	-0.10762(8)	-0.10727(12)
O1 (4e)					
z	0.15016(17)	0.15050(18)	0.14930(19)	0.14871(31)	0.14882(38)
O2 (4f)					
z	-0.05512(20)	-0.05586(22)	-0.05437(23)	-0.05481(33)	-0.05474(45)
O3 (6h)					
x	0.18875(89)	0.18568(110)	0.18268(104)	0.18262(118)	0.18194(187)
O4 (12k)					
x	0.15559(70)	0.15385(76)	0.15384(69)	0.15407(109)	0.15050(125)
z	0.05182(11)	0.05139(11)	0.05152(11)	0.05230(19)	0.05178(24)
O5 (12k)					
x	0.50339(92)	0.50423(100)	0.50556(89)	0.50557(151)	0.50839(164)
z	0.14909(8)	0.14891(8)	0.14848(9)	0.14801(14)	0.14784(19)
R_{wp}, %	9.08	8.55	11.1	15.2	23.5
R_{exp}, %	5.54	6.79	8.81	11.05	16.21
R_B, %	4.24	4.51	4.15	6.87	9.82
R_{Mag}, %	6.24	5.10	8.87	10.2	17.7
χ^2	2.69	1.59	1.60	1.88	2.11

The dependence of lattice parameters versus composition is shown at Fig. 2. The volume of unit cell of the Al-doped barium hexaferrite is lower than pure $BaFe_{12}O_{19}$ composition [28, 29].

While the aluminum ions concentration increases the volume of the unit cell is decreased. It is due to smaller ionic radii of the Al^{3+} ions (0.535 Å) unlike of the Fe^{3+} (0.645 Å) ions [30].

The quantitative phase analysis was determined from Rietveld refinement date using the following equation [31]:

$$W_j = \frac{S_j Z_j M_j V_j}{\sum_j S_j Z_j M_j V_j} \quad (2)$$

where Sj is the Rietveld scale factor, Zj is the number of formula units per unit cell, Mj is the formula unit molecular weight, Vj is the unit cell volume of the j-th phase and the index j in the summation is over all phases included in the model. According to our calculations, the weight percent of secondary phase is nearly 0.97-1.4 %.

The unit cell volume as well as lattice parameters (*a* and *c*) decrees with decreasing temperature (Fig. 2 insert). For a typical ferrite, the coefficient of linear thermal expansion, is calculated as:

$$\alpha_V = (1/L_0)(dL/dT) \quad (3)$$

Where L and L_0 are the lengths at temperature *T* and reference temperature T_0, respectively. The high anisotropy of crystal structure leads to difference of the coefficient of linear thermal expansion for *a* (α_a~9.32*10^{-6} [1/K]) and *c* (α_c~1.5*10^{-5} [1/K]) axis.

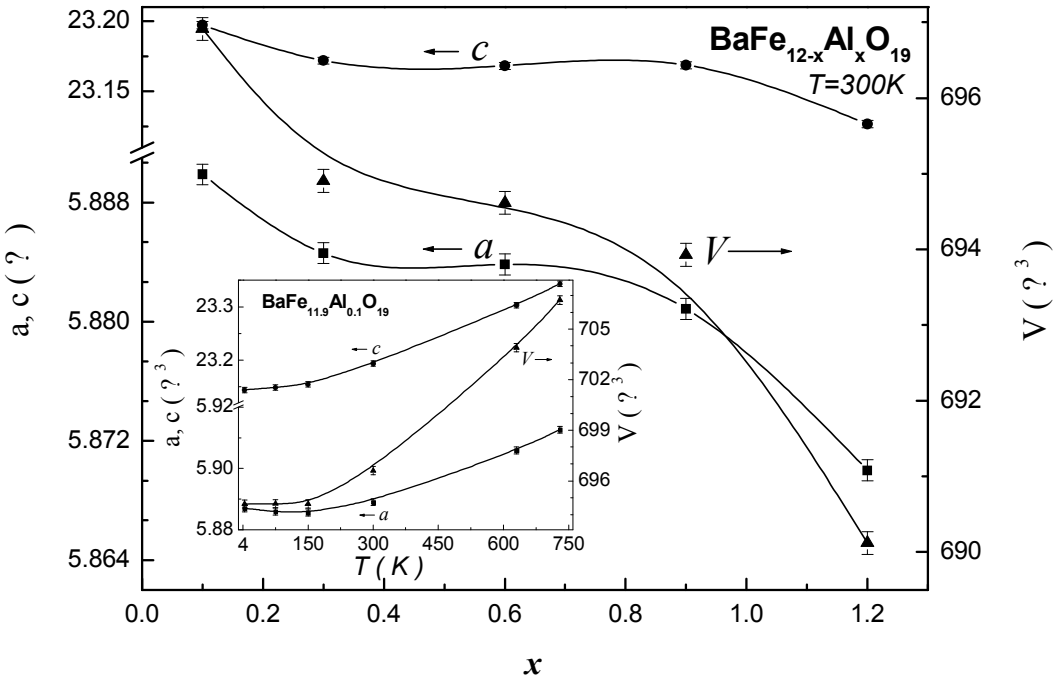

Fig. 2. The concentrational dependence of the refined (*a* and *c*) lattice parameters and *V* unit cell volume obtained by powder neutron diffraction at 300 K for the $BaFe_{12-x}Al_xO_{19}$ (x = 0.1 – 1.2) solid solutions. Insert demonstrates the temperature dependence of the refined (*a* and *c*) lattice parameters and *V* unit cell volume.

In low temperature range from 150 to 4.2 K the Invar effect (zero thermal expansion coefficient) is observed for all compositions. In this range decreasing temperature leads to low decrease of cell volume and c axis, whereas *a* axis increases. Fig. 2 insert shows temperature dependences for the $BaFe_{11.9}Al_{0.1}O_{19}$ where decreasing temperature leads to low decrease of cell volume at 0.002 $Å^3$, whereas c axis decreases at 0.01 Å and a axis increases at 0.001 Å (see Fig. 2). Similar dependences of lattice parameters versus low temperature are observed in steels [32], metallic oxides [33] and invar alloys [34]. It is well known, that the thermal extension are defined by lattice, electron and magnetic contributions. The lattice contribution gives main contribution at high temperature. The electron and magnetic contributions exceed the lattice contribution in low temperature region. The analysis of low temperature neutron reflexes denotes absence of changes in magnetic structure as distinct from invar alloys near the phase transition temperature. In our opinion the most credible explanation of the thermal expansion behavior in range from 150 to 4.2 K for the $BaFe_{12-x}Al_xO_{19}$ is the anharmonicity of low energy phonon modes, according to [35].

3.2. Microstructure

Fig. 3 demonstrates electron microscopy images of the $BaFe_{12-x}Al_xO_{19}$ ceramics. The samples represent a densely packed polycrystals (> 95%) with an average crystallite size till 200 nm. The variation in grain size is significant. The grains have identifiable manner with hexagonal plates cut.

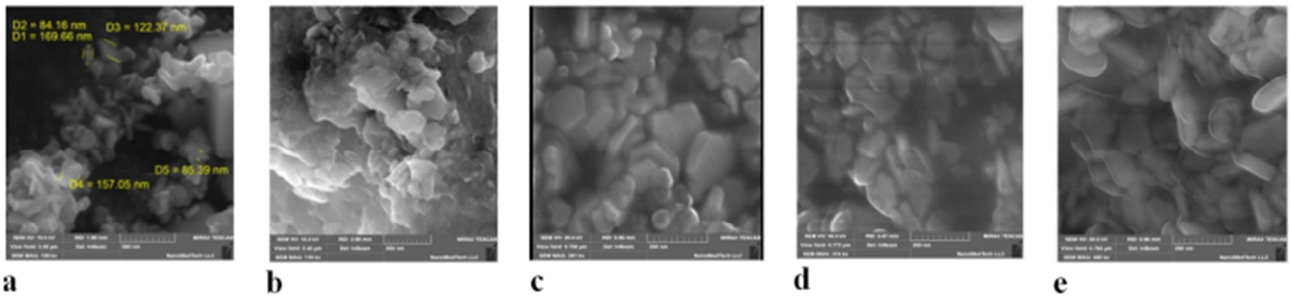

Fig. 3. The image of microstructure obtained by scanning electron microscopy for the $BaFe_{12-x}Al_xO_{19}$ (x = 0.1 – 1.2) solid solutions. a – x=0.1; b – x=0.3; c – x=0.6, d – x=0.9; e – x=1.2.

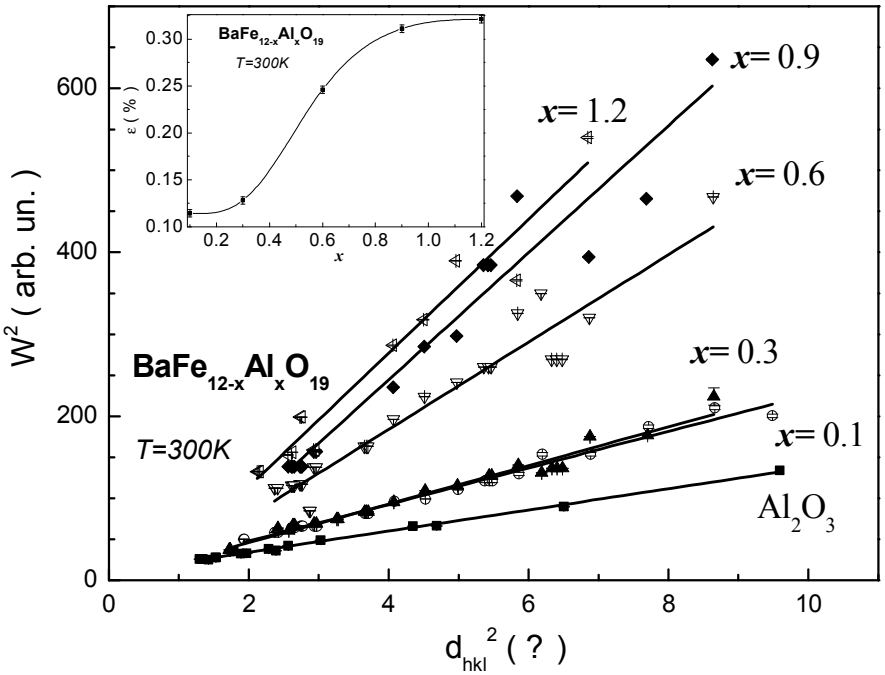

Fig. 4. The dependence of the full wide at half maximum square of diffraction peaks versus interplanar distance square at 300 K for the $BaFe_{12-x}Al_xO_{19}$ (x = 0.1 – 1.2) solid solutions. Insert demonstrates the concentrational dependence of microstraine.

The information about microstraine was obtained from the diffraction line broadening. The W^2 reflection-half-width square versus d^2 interplanar spacing square for the $BaFe_{12-x}Al_xO_{19}$ is shown at Fig. 4.

The line broadening of powder neutron diffraction pattern of Al-doped barium hexaferrites are increased with increasing of Al^{3+} ions concentration. The full wide at half maximum of neutron peak is described, according to [32, 35], by equation:

$$W^2 = C_1 + C_2 d^2 + C_3 d^2 + C_4 d^4 \qquad (4)$$

Where C_1, C_2, C_3, C_4 – refining constants; W – full wide at half maximum of diffraction peak; $(C_1+C_2d^2)$ – resolution function of HRFD obtained from standard Al_2O_3 (SRM-676 of NIST, USA); C_3d^2 – contribution determined by size effect; C_4d^4 – contribution determined by microstraine effect.

The contribution of the true physical line broadening of powder neutron peaks for the $BaFe_{12-x}Al_xO_{19}$ was determined by FullProf software calculated as difference of wide between experimental samples and standard Al_2O_3. The line broadening is connected with only microstresses factor. In ferrimagnetic crystals the separate sublattices give different contributions to general deformation. Besides, the local environment symmetry of magnetic ions in ferrimagnetic crystals differs from macroscopic symmetry. This leads to increase of the microscopic parameters number in comparison with microscopic. The slope of approximated function increases with increasing of the diamagnetic ion concentration. This behavior indicates that the microstraine increases in crystallites. It is shown in Fig. 4 the

experimental points correspond to different combinations of Miller indices, which indicates the absence of explicit anisotropic effects in the broadening of the diffraction peaks.

The dependence of microstraine value versus composition for the $BaFe_{12-x}Al_xO_{19}$ is shown at Fig. 4 insert. The calculation of microstraine values have performed for isotropic approximation i.e. (L > 3000 Å) size effect is absent. The minimum microstraine is observed in sample with x=0.1. The increase in the microscopic microstraine by increasing of the aluminum ions concentration associated with increasing of the system disorder, as a result of the statistical distribution of aluminum ions on magnetic sublattices, which can make different contributions to the total deformation.

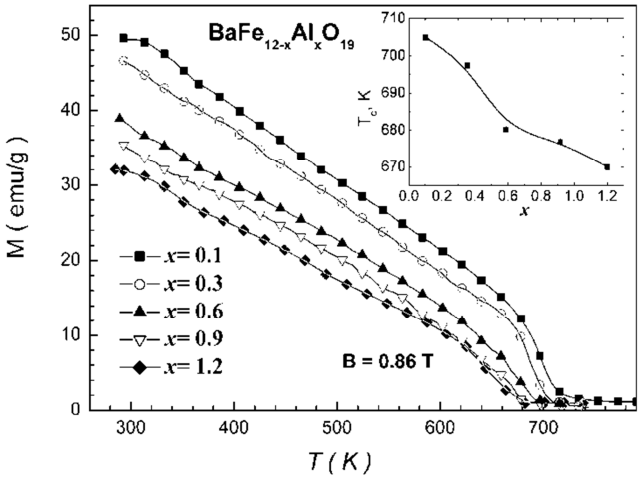

Fig. 5. The temperature dependence of the specific magnetization for the BaFe12-xAlxO19 (x = 0.1 – 1.2) solid solutions. Insert demonstrates Tc for each composition.

3.3. Magnetic Properties

Fig. 5 demonstrates temperature dependences of the specific magnetization for the $BaFe_{12-x}Al_xO_{19}$ obtained by VSM. Insert demonstrates T_c for each composition. According magnetic investigations the paramagnetic-ferrimagnetic T_c phase transition temperature for the $BaFe_{12-x}Al\ O_{19}$ is observed at temperature range 705-670 K. Whereas for pure $BaFe_{12}O_{19}$ the Curie temperature is equal 740 K [36, 37].

The increase in the concentration of aluminum ions leads to a reduction of the specific magnetization from 49.6 emu/g (x = 0.1) to 32 emu/g (x = 1.2) at room temperature. As the increase of the diamagnetic Al ions concentration in the solid solutions of barium hexaferrite, the number of neighbors of magnetically iron ions is reduced so that the magnetic order is destroyed at lower temperatures [38].

Such behavior of the specific magnetization (magnetization values decrease with increasing concentration of aluminum ions) is observed on the graph of the field dependence of the specific magnetization (Fig. 6). Almost all the samples go into saturation in external magnetic fields up to 0.2 T [39].

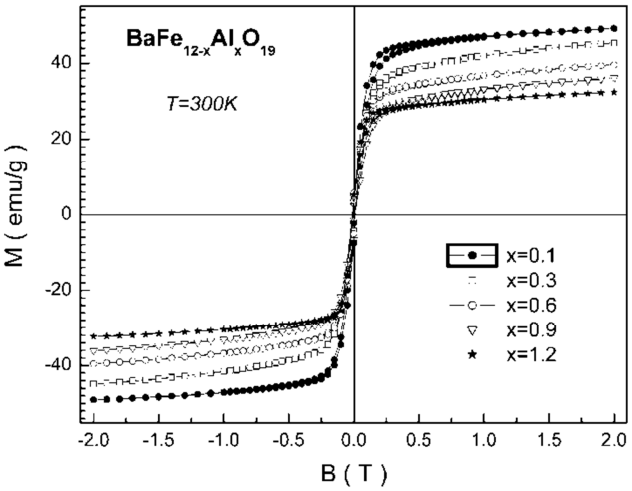

Fig. 6. The field dependence of the specific magnetization at 300 K for the $BaFe_{12-x}Al_xO_{19}$ (x = 0.1 – 1.2) solid solutions.

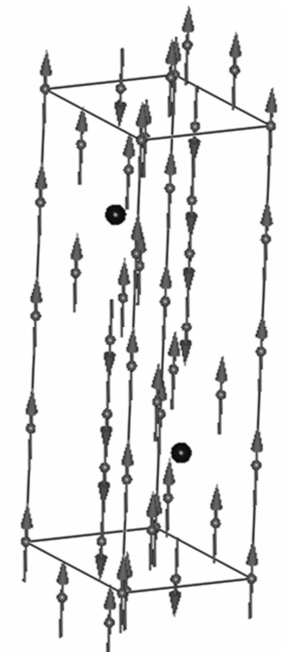

Fig. 7. The magnetic structure of the $BaFe_{12-x}Al_xO_{19}$ (Gorter model) at room temperature. Depicted Fe^{3+}ions (magnetic moment) and Ba^{2+} ions (without magnetic moment).

3.4. Magnetic Structure

In hexaferrites the magnetic Fe^{3+} ions are located in positions which have octahedral (Fe1-2a, Fe4-4f_{VI} and Fe5-12k), tetrahedral (Fe3-4f_{IV}) and bipyramidal (Fe2-2b) oxygen environment. As a result of partial replacement of iron ions by diamagnetic aluminum ions which are distributed statistically equivalent for all positions of the magnetic lattice it can be expected to change in the values of the magnetic moments in corresponding positions. The data were collected at room temperature, well below the phase transition temperature for ferrimagnetic-paramagnetic appropriate formulations. Its description in the concentration range from x = 0.1 to 1.2 fully satisfies the model proposed by Gorter

[40], according to which, all the magnetic moments of the atoms Fe^{3+} are oriented along the easy axis which coincides with the hexagonal axis *c* (Fig. 7).

Table 2 and Fig. 8 show the values of the concentration dependence of the magnetic moments of Fe^{3+} ions in different crystallographic positions: 2a, 2b, $4f_{IV}$, $4f_{VI}$ and 12k.

Table 2. The magnetic moment per iron ion in different positions obtained by powder neutron diffraction at 300 K for the $BaFe_{12-x}Al_xO_{19}$ (x = 0.1 – 1.2) solid solutions.

X	0.1	0.3	0.6	0.9	1.2
Fe1 (2a)	3.82	3.77	3.25(0.03)	3.36	2.16
Fe2 (2b)	4.08(0.13)	4.11(0.15)	3.09	3.74	2.18(0.19)
Fe3 ($4f_{IV}$)	3.65(0.09)	3.68(0.10)	3.25(0.11)	3.60(0.18)	1.47(0.08)
Fe4 ($4f_{VI}$)	4.09(0.09)	4.15(0.11)	3.75(0.03)	3.57(0.19)	1.25(0.09)
Fe5 (12k)	3.59	3.55(0.05)	3.25(0.03)	3.12(0.08)	2.07

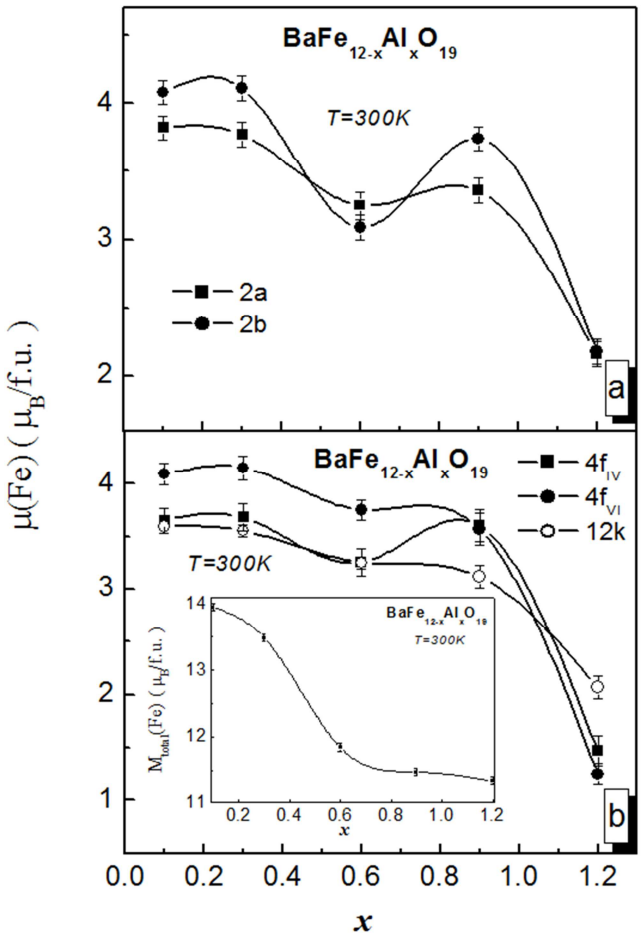

Fig. 8. The concentrational dependence of the magnetic moment per iron ion in different positions obtained by powder neutron diffraction at 300 K for the $BaFe_{12-x}Al_xO_{19}$ (x = 0.1 – 1.2) solid solutions. Insert demonstrates the concentrational dependence of the total magnetic moment per f.u.

As the substitution of iron ions by aluminum ions the exchange interaction between the magnetic sublattices is broken which leads to a decrease in the value of their magnetic moments. A slight change in the magnetic moment x = 0.6 composition appears to reduce the magnitude of the sublattice magnetic moments of the formed iron ions located at positions 2a and 2b may be due to inhomogeneities in the distribution of aluminum ions on crystallographic positions in the preparation of the samples.

It can be assumed that at a low concentration of aluminum ions in the compound it should be distributed statistically throughout nonequivalent positions magnetic hexagonal ferrite lattice. However in our case to reduce the discrepancy between the experimental data and performed calculations of the magnetic and crystal lattices for the Al-doped barium hexaferrites the aluminum ions in a greater degree was preferred to the substitution of iron ions into the 2a, 2b and 12k positions, while $4f_{IV}$ and $4f_{VI}$ - to a lesser degree. Since the Al ions distribution is largely influenced by the method of sample preparation, the confirmation of the correctness of our judgments on their distribution in the corresponding crystallographic positions is planned to be found in the course of further research.

Resulting or total magnetic moment per formula unit for the barium hexaferrite ($BaFe_{12}O_{19}$) at T temperature can be calculated according [41] to the formula:

$$M_{total}(T) = 1[m_{2a}(T)] + 1[m_{2b}(T)] - 2[m_{4fIV}(T)] - 2[m_{4fVI}(T)] + 6[m_{12k}(T)] \quad (5)$$

If the magnetic moment of Fe^{3+} ion at 0 K is equal $5\mu_B$ then magnetic moment of pure $BaFe_{12}O_{19}$ ferrite will be equal to $20\mu_B$ per formula unit. The total magnetic moment (M_{total}) for the $BaFe_{12-x}Al_xO_{19}$ solid solutions is shown at Fig. 8 insert. Such low values are explained by influence of diamagnetic Al ions and thermal factor causing the disorientation of the magnetic moments in space due to the increase of the thermal fluctuations of the ions forming the crystal lattice.

4. Conclusions

By high resolution neutron diffraction over a wide concentration range was investigated behavior of the crystal and magnetic structures of samples of the $BaFe_{12-x}Al_xO_{19}$ solid solutions. The temperature and field dependences of specific magnetization was investigated by VSM. It is shown that the magnetic structure of the samples over the entire range of concentrations in good agreement with Gorter's model according to which the magnetic moments of the Fe^{3+}

ions are oriented along the hexagonal axis is the axis of easy magnetization. The observed decrease in the Curie temperature with increasing of diamagnetic ions concentration due to the weakening of the Me-O-Me exchange interaction i.e. number of neighbors of magnetic iron ions is reduced so that the magnetic order is destroyed at lower temperatures. This causes the decrease of T_C and reduction of the specific magnetization from 49.6 emu/g (x = 0.1) to 32 emu/g (x = 1.2) at room temperature with increasing in the concentration of aluminum ions.

When the concentration of aluminum ions increases in the crystallites the microstrain increases that can be attributed to the increasing of the system disorder as a result of the statistical distribution of the aluminum ions of the magnetic sublattices, having a smaller ionic radius unlike iron ions.

Acknowledgement

The work was carried out with financial support in part from the Ministry of Education and Science of the Russian Federation in the framework of Increase Competitiveness Program of NUST «MISiS» (№ K4-2015-040). L.V. Panina acknowledges support under the Russian Federation State contract for organizing a scientific work.

References

[1] P.A. Marinõ-Castellanos, J. Anglada-Rivera, A. Cruz-Fuentes, R Lora-Serrano, J. Magn. Magn. Mater. 280 (2004) 214.

[2] P.A. Marinõ-Castellanos, A.C. Moreno-Borges, G. Orozco-Melgar, J.A. García, E. Govea-Alcaide, Physica B 406 (2011) 3130.

[3] I. Bsoula, S.H. Mahmood, J. Alloys Compd. 489 (2010) 110.

[4] Y. Du, H. Gao, X. Liu et, J. Wang, P. Xu, X. Han, Journal of Materials Science 45 (2010) 2442.

[5] V.A. Turchenko, A.V. Trukhanov, I.A. Bobrikov, S.V. Trukhanov, A.M. Balagurov, J. Surf. Investig. 9 (2015) 17.

[6] V. Adelskold, Avk. Miner. A 12 (1938) 1.

[7] R.N. Summergard, E. Banks, J. Phys. Chem. Solids 2 (1957) 312.

[8] S. Diaz-Castañón, J.L. Sánchez, L. I. Estevez-Rams, F. Leccabue, B.E. Watts, J. Magn. Magn. Mater. 185 (1998) 194.

[9] M. Isshiki, T. Suzuki, T. Ito, T. Ido, T. Fujiwara, IEEE Transactions on Magnetics 21 (1985) 1486

[10] S. Bierlich, T. Reimann, H. Bartsch, J. Töpfer, J. Magn. Magn. Mater. 384 (2015) 1.

[11] N. Hur, S. Park, P.A. Sharma, J.S. Ahn, S. Guha, S.W. Cheong, Nature 429 (2004) 392.

[12] S. Ryu, J.Y. Kim, Y.H. Shin, B.G. Park, J.Y. Son, H.M. Jang, Chem. Mater. 21 (2009) 5050.

[13] N. Ikeda, H. Ohsumi, K. Ohwada, K. Ishii, T. Inami, K. Kakurai, Y. Murakami, K. Yoshii, S. Mori, Y. Horibe, H. Kito, Nature 436 (2005) 1136.

[14] M. Wang, G.L. Tan, Mater. Res. Bull. 46 (2011) 438.

[15] G.L. Tan, M. Wang, Journal of Electroceramics 26 (2011) 170.

[16] P. Hemberger, P. Lunkenheimer, R. Fichtl, H.A. Krug von nidda, V. Tsurkan, A. Loidl, Nature 434 (2005) 364.

[17] G. Tan, X. Chen, J. Magn. Magn. Mater. 327 (2013) 87.

[18] Y. Tokunaga, Y. Kaneko, D. Okuyama, S. Ishiwata, T. Arima, S. Wakimoto, K. Kakurai, Y. Taguchi, Y. Tokura, Phys. Rev. Lett. 105 (2010) 257201.

[19] G.D. Nipan, V.A. Ketsko, A.I. Stognij, A.V. Trukhanov, T.N. Kol'tsova, M.A. Kop'eva, L.V. Elesina, N.T. Kuznetsov, Inorganic materials, 46 (2010) 429.

[20] S.V. Trukhanov, A.V. Trukhanov, S.G. Stepin, H. Szymczak, C.E. Botez, Phys. Solid State 50 (2008) 886.

[21] S.V. Trukhanov, A.V. Trukhanov, C.E. Botez, A.H. Adair, H. Szymczak, R. Szymczak, J. Phys.: Condens. Matter. 19 (2007) 266214.

[22] S.V. Trukhanov, A.V. Trukhanov, A.N. Vasil'ev, A. Maignan, H. Szymczak, JETP Letters 85 (2007) 507.

[23] H.M. Rietveld, Journal of Applied Crystallography 2 (1969) 65.

[24] http://www.ill.eu/sites/fullprof/.

[25] V.N. Dhage, M.L. Mane, A.P. Keche, C.T. Birajdar, K.M. Jadhav,Physica B 406 (2011) 789.

[26] I. Bsoul and S.H. Mahmood, Jordan Journal of Physics 2 (2009) 171.

[27] A.C. Larson, R.B. Von Dreele, LANL Report LAUR 86 (2000).

[28] Ashima, S. Sanghi, A. Agarwal, Reetu, J. Alloys Comp. 513 (2012) 436.

[29] J. Wang, F. Zhao, W. Wu, G.-M. Zhao, J. Appl. Phys. 110 (2011) 096107.

[30] R.D. Shannon Acta Crystallographica A 32 (1976) 751.

[31] A.L. Ortiz, F. Sánchez-Bajo, A. Hernández-Jiménez, F. Guiberteau, F.L. Cumbrera, J. Eur. Ceram. Soc. 22 (2002) 2677.

[32] V.V. Sumin, V.G. Simkin, S.G. Sheverev, M.V. Leont'eva-Smirnova, V.M. Chernov The Physics of Metals and Metallography 108 (2009) 600.

[33] T. Chatterji, T.C. Hansen, M. Brunelli, P.F. Henry, Appl. Phys. Lett. 94 (2009) 241902.

[34] G.K. White, Proceedings of the Physical Society 86 (1964) 159.

[35] G. D. Bokuchava, A.M. Balagurov, V.V. Sumin, I.V. Papushkin, J. Surf. Investig. 4 (2010) 879.

[36] T. Tsutaoka, N. Koga, J. Magn. Magn. Mater. 325 (2013) 36.

[37] B.T. Shirk, W.R. Buessem, J. Appl. Phys. 40 (1969) 1294.

[38] S.V. Trukhanov, JETP 100 (2005) 95.

[39] S. V. Trukhanov, A.V. Trukhanov, A.N. Vasiliev, A.M. Balagurov, H. Szymczak, JETP 113 (2011) 820.

[40] E. W. Gorter, Proc. IEEE Suppl. 104B, 225 (1957).

[41] J. Smit, H.P.J. Wijn Ferrites. Cleaver – Hume Press Ltd. (1959), p. 142.